PROCEEDINGS A

rspa.royalsocietypublishing.org

Research

Article submitted to journal

Subject Areas:
xxxxx, xxxxx, xxxx

Keywords:
xxxx, xxxx, xxxx

Author for correspondence:
D. Rayneau-Kirkhope
e-mail:
daniel.rayneau-kirkhope@aalto.fi

Analytic analysis of auxetic metamaterials through analogy with rigid link systems

Daniel Rayneau-Kirkhope[1,2], Chengzhao Zhang[2,3], Louis Theran[2,4], Marcelo A. Dias[2,5]

[1]Department of Applied Physics, Aalto University, FI-02150 Espoo, Finland
[2]Aalto Science Institute, Aalto University, FI-02150 Espoo, Finland
[3]Department of Mathematics, Massachusetts Institute of Technology, USA
[4]School of Mathematics and Statistics, University of St Andrews, St Andrews KY16 9SS, Scotland, UK
[5]Department of Engineering, Aarhus University, Inge Lehmanns Gade 10, 8000 Aarhus C, Denmark

In recent years many structural motifs have been designed with the aim of creating auxetic metamaterials. One area of particular interest in this subject is the creation of auxetic material properties through elastic instability. Such metamaterials switch from conventional behaviour to an auxetic response for loads greater than some threshold value. This paper develops a novel methodology in the analysis of auxetic metamaterials which exhibit elastic instability through analogy with rigid link lattice systems. The results of our analytic approach are confirmed by finite element simulations for both the onset of elastic instability and post-buckling behaviour including Poisson's ratio. The method gives insight into the relationships between mechanisms within lattices and their mechanical behaviour; as such, it has the potential to allow existing knowledge of rigid link lattices with auxetic paths to be used in the design of future buckling induced auxetic metamaterials.

1. Introduction

The response of a structure to an external mechanical stimulus is often a direct consequence of the structure's geometry; thus it is reasonable to expect that with

THE ROYAL SOCIETY PUBLISHING

adaquate control of a material's architecture, it is possible to design a material's substructure to yield a given mechanical reponse [1]. This category of structure, where geometry rather than material properties govern the macroscopic response of a solid, are termed "mechanical metamaterials" [2–4]. Perhaps the most well-known class of mechanical metamaterials are those with an auxetic reponse to external load [5,6]. Such structures, when compressed (stretched), contract (expand) in the direction perpendicular to the applied load. Auxetic behaviour has been observed in layered ceramics [7], foams [9] and re-entrant foams [5,10], origami [4,11,12] and kirigami [13,14] geometries, structures with rotating elements [15–18], dimpled sheets [19], and other carefully designed architectures [20–24].

Some auxetic materials are part of an emerging paradigm whereby the use of elastic instability is viewed as a route to new functionality rather than a mode of failure [25–29]. In auxetic metamaterial based on this concept, (as suggested in [30], and later experimentally realised [31–34]) spontaneous symmetry breaking associated with buckling creates an ordered collapse of the structure. Such architectures exhibit conventional behaviour (positive Poisson's ratio) prior to buckling and make a transition to auxetic behaviour at the buckling load [31–34]. Most works focused on auxetic properties created through the buckling of periodic cellular structures focus on numerical or experimental methods [35]. The few existing analytic investigations on this subject focus on elastic stability of the lattices through the application of beam theory [35–38] and investigate only the onset of elastic instability. Beam theory based methodologies are poorly suited to the geometry considered here due to the non-uniform nature of the lattice elements and the low aspect ratios in certain regions of the lattice. There is a substantial body of work using algebraic-geometric techniques to determine whether a specific deformation of a rigid link geometry is auxetic [21,39–42], provided the geometry is sufficiently non-singular. Our interest here is in symmetry breaking and associated auxetic paths; we start with a singular configuration and using a novel approach, predict how the structure will leave this initial state.

In this paper, using a novel methodology, we analyse the buckling induced auxetic behaviour of a continuum lattice through analogy with systems made from rigid links and torsional springs. Our methodology allows us to analytically investigate the spontaneous symmetry breaking of an initially singular lattice of rigid links. Furthermore, we demonstrate a fundamental connection between the buckling-induced auxetic response of a lattice made up of a soft material and the mechanisms ("floppy modes") designed into a lattice of rigid links. This approach yields concise analytic expressions for the buckling load, postbuckling path and Poisson's ratio of the continuum structure, giving insights into the fundamental mechanics of the system, and reducing the computational cost of investigations. We present confirmation of our analytic methods through finite element methods on the continuum structure. In order to facilitate the analogy between rigid link and continuum based structures, we utilise a specific void shape in the continuum lattice, allowing the straightforward calculation of the appropriate values for the torsional springs in the rigid link system. We stress, however, that although the mechanics of lattices are heavily dependent on the lattice connectivity [43,44], for an elastomer with an array of voids arranged on a square lattice, the underlying mechanisms within the lattice structure are relatively insensitive to the nature of the voids [45]; thus we hypothesise that the rigid-link analysis proposed here elucidates the fundamental mechanisms present within a wide range of elastic instabilities in lattice based materials.

2. Lattice stability

The deformation of the rigid link lattice presented in Fig. (1, left) is parameterised by a set of angles $\{\theta_{i,j}\}$ denoting the rotation of the initially vertical elements, while another set of angles $\{\eta_{i,j}\}$ is used to represent the rotations of the initially horizontal elements. The indices i and j take integer values and denote the position of the element: element (i, j) has its centre initially positioned at (iL, jL) where L is the length of the links. There are no horizontal element on the upper and lower boundaries ($j = 0, N_y$). The energy of any deformation described by the

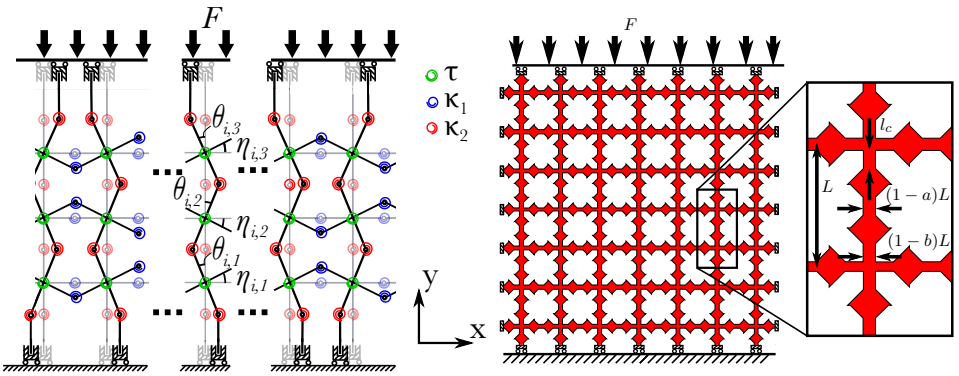

Figure 1. Left: The rigid link lattice is comprised of infinitely stiff members connected by rotational springs. At the hinges, between two neighbouring links, springs of stiffnesses κ_1 and κ_2 are placed. Where two links overlap, they are assumed to be pin jointed, rotation relative to one another is permitted at the expense of deforming a torsional spring of stiffness τ. Right: An analogous continuum lattice is shown, where red indicates a soft elastomer while white shows the voids. The notation L, a, b and l_c make reference to various quantities describing the continuum lattice, this notation is indicated in the inset to the figure. The boundary conditions are shown schematically in the diagram – on the horizontal boundaries the free ends of the lattice are assumed to translate in the y direction together, while translations in the x direction are free. On the vertical boundaries translation of the free ends in both the x and y direction are permitted. On both boundaries, rotations are not permitted.

parameters $\{\theta_{i,j}, \eta_{i,j}\}$ can be calculated as,

$$U = \sum_{i=1}^{N_x}\sum_{j=0}^{N_y} \frac{\kappa_1\left(1+\delta_{j,1}+\delta_{j,N_y}\right)}{2}\left(\theta_{i,j+1}-\theta_{i,j}\right)^2 + \sum_{i=1}^{N_x}\sum_{j=1}^{N_y}\frac{\tau}{2}\left(\theta_{i,j}-\eta_{i,j}\right)^2 + \sum_{i=1}^{N_x-1}\sum_{j=1}^{N_y}\frac{\kappa_2}{2}\left(\eta_{i+1,j}-\eta_{i,j}\right)^2 - \sum_{i=1}^{N_x}\frac{Fl}{N_x}\sum_{j=1}^{N_y}\left(1-\cos\theta_{i,j}\right), \tag{2.1}$$

where κ_1, κ_2 and τ are the stiffnesses of the torsional springs in the system (springs with stiffness κ_1 (κ_2) penalise rotation of initially vertical (horizontal) elements relative to their neighbours while τ springs penalise relative rotation of the vertical and horizontal elements whose centres remain coincident). The term proportional to κ_1 contains the Kronecker delta function $\delta_{i,j}$ to account for our choice of boundary constraints. The last term in Eq. (2.1) is the external work done on the system by the force F. Due to the connectivity of the lattice and fixed length of elements, we impose a set of constraints. Working to first order in $\{\theta_{i,j}, \eta_{i,j}\}$, it can be shown that for a deformation to be compatible with the connectivity of the lattice, the distance between the locations of $\eta_{i,j}$ and $\eta_{i+1,j}$ takes a constant value for all j. Furthermore it is required that

$$\eta_{i,j} = -\eta_{i+1,j}. \tag{2.2}$$

We set the boundary conditions of the system to be,

$$\theta_{i,0} = -\theta_{i,1}, \tag{2.3}$$

$$\theta_{i,N_y+1} = -\theta_{i,Ny}. \tag{2.4}$$

(a) Symmetry relations

Here we introduce the condition that the deformation mode of a vertical column of rigid links ($\theta_{i,j}$) will be related to that of its neighbour ($\theta_{i+1,j}$), through one of two symmetry relations. Utilising standard group theoretic arguments [46] and assuming a lattice that is infinite in the x

direction, it can be shown [37,47] that the energy of the system is minimised when one of two symmetry relations is present:

$$\theta_{i,j} = \theta_{i+1,j}, \tag{2.5}$$

$$\theta_{i,j} = -\theta_{i+1,j}. \tag{2.6}$$

These modes will be referred to as translationally symmetric and mirror symmetric modes, respectively (these modes correspond to the sway and non-sway modes respectively of [38,48]). In the following subsections, we establish the buckling behaviour of the system subject to these two possible symmetry relations.

(i) Translational symmetry

Utilising the symmetry relationships presented above, the energy of a given deformation can be greatly simplified. In the case of translational symmetry ($\theta_{i,j} = \theta_{i+1,j}$) we see that energy minimisation with respect to $\eta_{i,j}$ enforces that

$$\eta_{i,j} = 0 \quad \forall \quad i, j. \tag{2.7}$$

Working to first order in $\theta_{i,j}$, direct calculation shows that the minimum energy configuration exists when

$$(2\kappa_1 + \tau - Fl)\theta_{n,m} - \kappa_1(\theta_{n,m+1} + \theta_{n,m-1}) + (\delta_{m,1} + \delta_{m,Ny})2\kappa_1 = 0 \tag{2.8}$$

is satisfied for all values of n and m. This requirement can be rewritten in matrix form,

$$\mathbf{A}\Theta = \mathbf{0} \tag{2.9}$$

where $\Theta = (\theta_{i,1}, \theta_{i,2}, ..., \theta_{n,N_y})^T$. It is noted that in matrix form the first two terms of Eq. 2.8 create a tridiagonal symmetric Toeplitz matrix, the remaining term means that the full expression for $\mathbf{A}$ deviates slightly from this form. Buckling of the system into a mode with translational symmetry will occur if the loading on the system is sufficient to create (at least) one zero eigenvalue of $\mathbf{A}$. For suitably large values of N_y, neglecting the last term in Eq. (2.8) yields a good approximation to the system (for physically relevant parameters here, $N_y > 5$ is sufficient). This approximation allows for an analytic solution to the eigenvalue problem. We find that buckling of the system into a mode with translational symmetry will occur if the loading on the system exceeds the threshold

$$F_{\text{min}} = \frac{2\kappa_1 + \tau - 2\kappa_1 \cos\left(\frac{\pi}{N_y+1}\right)}{l}, \tag{2.10}$$

and the associated mode is found to be

$$\Theta_i = A \sin\left(\frac{i\pi}{n+1}\right). \tag{2.11}$$

For small values of N_y, the eigenmode of this system can be obtained numerically.

(ii) Mirror symmetry

The second symmetry between neighbouring columns we consider here is that of mirror symmetry ($\theta_{i,j} = -\theta_{i+1,j}$). Due to the restriction that the mid-point of vertical and horizontal bars are coincident throughout the deformation process, it can be shown that,

$$\theta_{i,j} = \pm\theta \tag{2.12}$$

for some value of θ and that the sign of any rotation in the lattice is the opposite of its nearest neighbours. Furthermore through the minimisation of energy with respect to η, we also derive an

expression for the rotation of initially vertical elements:

$$\eta_{i,j} = \gamma(N_x, \tau, \kappa_2)\theta_{i,j}, \tag{2.13}$$

where γ is a constant depending on the lattice geometry. The energy of the whole system for a given deformation can then be expressed as

$$U = \Omega\theta^2 - FLN_y(1 - \cos\theta) \tag{2.14}$$

for some Ω which depends on parameters describing the lattice. Working to first order in θ, we can thus establish that the minimum energy configuration corresponds to non-zero values of θ (buckled configurations), provided F is above

$$F_{\text{min}} = \frac{2\Omega}{N_x N_y l}. \tag{2.15}$$

3. Rigid link as a continuum approximation

If we now consider a continuum lattice structure, as shown in figure 1 (right), the slender beams within the framework serve as hinge points when the lattice deforms beyond the buckling threshold. The resistance to bending of these slender beams is easily obtainable and, thus, we are able to calculate the effective values of κ_1, κ_2 and τ of the continuum lattice. From standard beam theory [49], it can be found that the appropriate stiffnesses of these springs are given by

$$\kappa_1 = \kappa_2 = \frac{EI_\kappa}{l_c} \tag{3.1}$$

$$\tau = \frac{2EI_\tau}{l_c}, \tag{3.2}$$

where E is the Young's Modulus of the material, I_κ and I_τ are the second moment of area of the slender elements making up the κ_1, κ_2 and τ springs and l_c is the length of the slender elements. Therefore, using the expressions for buckling of the rigid link lattice found in the previous section, we can predict the buckling load of the more complex continuum lattice system.

(a) Linear stability

From the two predicted buckling loads derived for the rigid link lattice presented in section 2 (Eqs. (2.10 & 2.15)), with above expressions relating the continuum lattice geometry to the rigid link structure (Eqs. (3.1 & 3.2)), we are able to derive two possible loading values for the continuum structure that will mark the onset of instability. The minimum value of the two buckling loads of the lattice (corresponding translational or mirror symmetry) will be the physically relevant mode. These predictions are shown in figure 2, where confirmation is obtained through finite element methods. Increasingly good quantitative match is found for more slender beam elements. The form of the buckling modes, as predicted in Eqs. (2.11, 2.12 & 2.13) are confirmed through comparison with linear buckling studies undertaken through finite element studies on the continuum lattice, as shown in figure 3.

Through this analytic method, we are able to quickly explore the design space: we show the results for a parametric sweep of a and b (for fixed N_x, N_y, l_c and L) in figure 4 separating the design space into regions that will exhibit modes with mirror symmetry (lower right region of figure 4, mode shown in figure 3 (right)) and translational symmetry (upper left region of figure 4, mode shown on the left of figure 3). We confirm this boundary through finite element simulations on the continuum structure on either side of the boundary, see figure 4. It is noted that greater accuracy is observed between the method presented here and the results of finite element simulation for increased slenderness of beam elements ($(1-a)L/l_c \ll 1, (1-b)L/l_c \ll 1$); for the methodology presented here to be valid, N_y must be sufficiently large for the approximation used in the derivation of Eq. (2.10) to hold ($N_y > 5$), and N_x must be sufficiently large for the assumptions of symmetry to hold ($N_x > 6$).

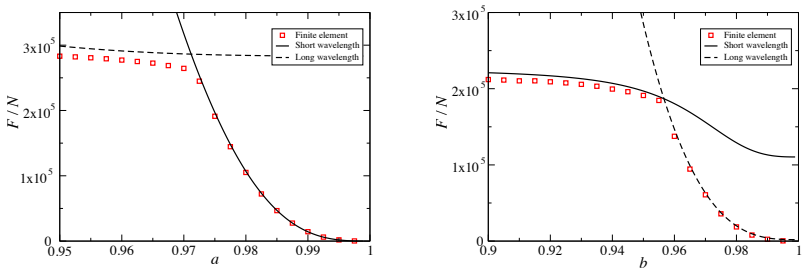

Figure 2. Comparison between finite element simulations and the analytic results derived in Eqs. 2.10 & 2.15. Both plots show results found for parameters $N_x = 10, N_y = 9$, $l_c = 3.75$mm and $L = 20$mm, τ and κ_n are given in Eq. (3.1 & 3.2). Left: The load at which elastic instability occurs for a parametric sweep of a with constant $b = 0.95$. Right: The load at which elastic instability occurs for varying b, with constant $a = 0.975$.

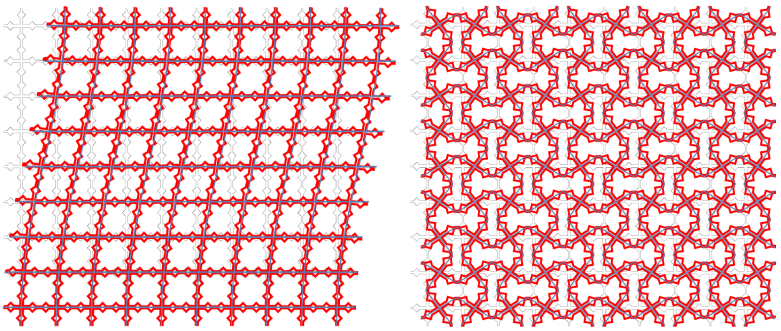

Figure 3. The comparison between linear buckling mode as predicted by the rigid link method (grey line) and the finite element work (red outline). Left showing the mode with translational symmetry, right with mirror symmetry. Here, the parameters used are $N_x = 10, N_y = 9, L = 20$mm, $l_c = 3.75$mm, $b = 0.92$ and $a = 0.945$ (left) and $a = 0.96$ (right).

(b) Postbuckling

The postbuckling of the rigid lattice can also be described analytically. Beyond the buckling threshold, due to the incompressibility of the links, the system remains in a configuration closely approximated by the modes predicted by the linear analysis [20]. The magnitude of these modes can be predicted through energy considerations. Substituting Eq. (2.11) or Eqs. (2.12 & 2.13) into Eq. (2.1), for the translationally symmetric or mirror symmetric mode respectively, we find that in both cases the energy of the system can be expressed as,

$$U \approx (\alpha_i - F\beta_i)B^2 + \zeta_i F B^4, \tag{3.3}$$

where B characterises the magnitude of deformation present within the system (in the case of a translationally symmetric mode, $B = A$ from Eq. (2.11), while for the mode with mirror symmetry, $B = \theta$ from Eq. (2.12)), α_i, β_i and ζ_i are constants that take values dependent on the mode being investigated. It can then be shown that the minimum energy configuration is realised as

$$B = \begin{cases} 0 & \text{for} \quad F < F_{\text{min}} \\ \sqrt{\frac{\alpha_i - F\beta_i}{2\zeta_i F}} & \text{for} \quad F > F_{\text{min}} \end{cases} \tag{3.4}$$

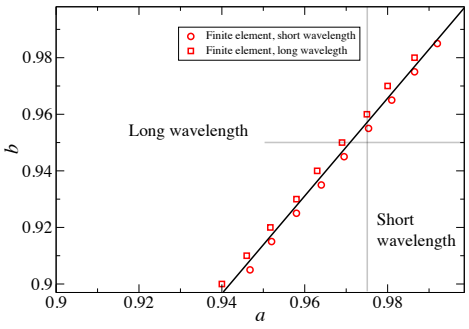

Figure 4. The predicted failure mode for the continuous system for varied values of a and b for fixed $N_x = 10, N_y = 9$, $l_c = 3.75$mm and $L = 20$. The black line separates the two modes as predicted by the rigid link model and red squares and circles are finite element confirmation of the boundary showing long and short wavelength modes respectively. Figure 2 can be thought of as a slices through this (a, b) space with an added axis of F (the load causing the onset of elastic instability) going out of the page. The grey lines show the region of phase space explored in figure 2.

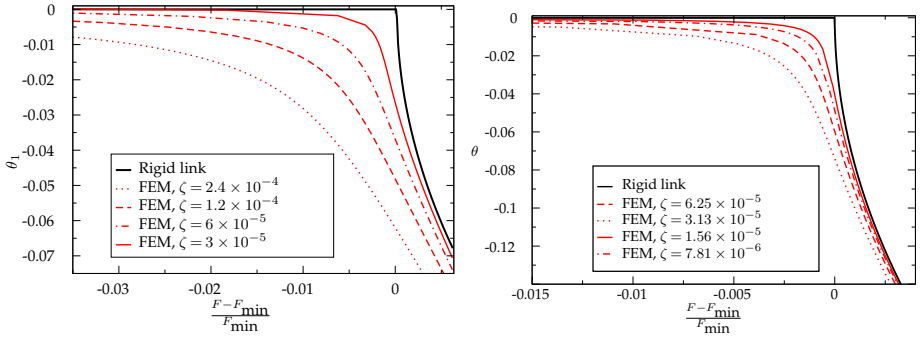

Figure 5. The perfect rigid link lattice acts as a limit for the continuum lattice with decreasing imperfections. Above shows the postbuckling behaviour of the continuum lattice found through FEM simulations for decreasing initial imperfection size in red for a mode with translational symmetry (left, $a = 0.945, b = 0.92$) and mirror symmetry (right, $a = 0.96, b = 0.92$), while the black curves show the postbuckling behaviour for a lattice of the same geometry predicted through Eq. (3.4) with appropriate parameters of τ and κ_n. It is noted that the value of F_{min} used in Eqs. (3.4) is taken from FEM simulations to correct for the error shown in figure 2. Other parameters used are given in caption of figure 3. Imperfections of varying magnitude were added to the structure in the form of the first eigenmode as predicted through the linear buckling analysis. In the case of the translationally symmetric mode (left) ζ represents the initial value of θ_1, in the mirror symmetric case (right), ζ gives the initial value of θ.

Thus, considering Eqs. (3.1 and 3.2), we make predictions about the nature of the postbuckling behaviour of the continuum lattice presented in figure 1. These predictions, alongside the postbuckling behaviour found through finite element simulations are shown in figure 5, where it is noted that the rigid link analysis appears as a limit to which the continuum lattice converges in the limit of decreasing magnitudes of imperfections in the system. In figure 1, the value of F_{min} used in Eq. (3.4) has been taken from the finite element simulations to decrease the error (these errors can be seen in figure 2).

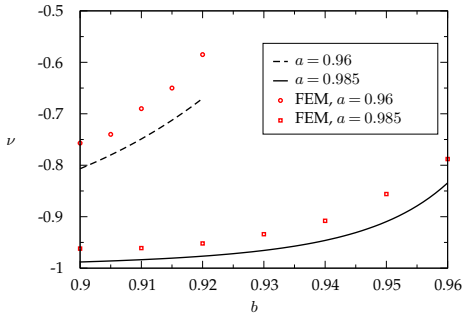

Figure 6. Points show the minimum Poisson's ratio exhibited by the continuum lattice for a lattice with $N_x = 10$, $N_y = 9$, $L = 20$mm and $l_c = 3.75$mm (results obtained by FEM). The black curves show the Poisson's ratio of the analagous rigid link lattice. Increasingly good agreement is found for increasing a and decreasing b.

(c) Auxetic behaviour

In the case of the rigid link structure, when the mirror symmetry mode is observed, the Poisson's ratio of the meta-material will be given by,

$$\nu = -\frac{1-\cos(\theta)}{1-\cos(\gamma\theta)}, \tag{3.5}$$

where the value of θ is given by Eq. (3.4), thus, for all deformations with this symmetry, the meta-material will be auxetic. The antisymmetric mode of the continuum system is also strongly associated with auxetic behaviour [31–34], where the Poisson's ratio of the structure is a function of the loading parameter [31]. We stress that in the limit of large deformations, in many cases, this dependence has a well defined limit (as investigated in [31]). By utilising the rigid link system, we are able to obtain estimates for this limit. For the geometry investigated here, it is found that, for large strains, localisation of deformations occur close to the boundaries. In figure 6 we plot the minimum value of the Poisson's ratio observed in FEM simulations (observed immediately before the localisation of deformation) and the Poisson's ratio predicted the rigid link analysis for various values of a and b (the parameters of the system are given in the caption of figure 3). It is observed that the error increases with increasing b and decreasing a. We observe that in these systems, localisation occurs earlier in the loading process, with increasing loading, the Poisson's ratio is observed to decrease [31], and thus earlier localisation contributes to larger observed errors. The larger the ratio a/b also leads to less bending in the node area of the continuum structure, this contributes to a difference in the Poisson's ratio of the rigid link lattice and its continuum counterpart.

4. Conclusion and Outlook

In this paper, we have elucidated the fundamental mechanisms behind the auxetic behaviour of a broad class lattice based metamaterials, and presented a new methodology in the analysis of such materials. We have applied symmetry arguments to simplify the problem before finding fully analytic solutions for the behaviour of the rigid link lattice for the onset of elastic instability and the post-buckling response. We have confirmed the applicability of our analytic findings on the rigid link lattice to the buckling induced auxetic lattice made from soft isotropic material through the comparison with finite element studies, including linear stability studies and post-buckling results. While in this work we have focused on the auxetic properties of the lattices, the methodology is well suited to the analysis of materials exhibiting frustrated mechanics and hysteretic behaviour. We hypothesise that the methodology presented here can be a useful tool

in the design of structures with the mechanical response programmed into the geometry of the material.

The methodology presented here gives fully analytic descriptions to complex lattice based meta-materials. While in this paper we have choosen to focus on the auxetic properties of lattice based materials, our approach can be applied to more complex lattice problems, including mechanical hysteresis and/or frustrated mechanics [50,51]. Such behaviour can be studied through the introduction of more complex mechanisms which permit further degrees of freedom and/or constraints within the rigid-link lattice. Furthermore, the adaptation of this method to include pore size/shape that vary with position in the lattice present an attractive and realistic goal. Such a methodology represents an important step in the development of stochastic and self assembled meta-materials, and the analysis of structures subject to manufacturing imperfections [52]. The analysis of such a system, where stochastic perturbations of geometry vary in space would require the modification or removal of the symmetry relations in section 2(a). The methodology presented here is increasingly accurate in the limit of large system sizes, in this same limit, finite element studies become computationally expensive. It is therefore hypothesised that this work may be of considerable use when working with systems where the pore size is much smaller than the dimension of the meta-material.

Similar mechanical systems based on rigid links and linear springs have been used to illucidate the fundamental physics of sytems such as auxetic behaviour of zeolites [53,54] and the anomolous elastic properties of some dielectric materials [55]; given the simplicity of the method developed here, and its accuracy in predicting phenomena of more complex structures, it is hoped that this method will shed yield insights on other systems. The work presented is based on the combination of well established fields of rigidity theory and elasticity, we hope that further interdisciplinary works can build on the wealth of knowledge in the two fields.

5. Appendix: FEM methods

Finite element studies were undertaken using COMSOL Multiphysics 5.2 [56]. In all cases, finite element work has considered the whole of the sample with N_x by N_y unit cells with boundary conditions as described below. Both the linear buckling analysis and quasi-static loading studies were performed on the same mesh. The mesh density varied depending on the aspect ratio of the members considered, however approximately 200 - 1500 mesh elements were used per unit cell. Mesh refinement studies were undertaken to check for convergence of results. In all simulations linear elastic materials were used, with a Young's Modulus of 170MPa and Poisson's ratio of 0.25. We used linear buckling analyses for results shown in figures 2, 3 and 4, and quasi-static studies with incremental loading for figure 5 and 6.

In the case of the linear buckling studies, a vertical load placed on the upper and lower boundaries of the system, these boundaries were permitted to translate in the x-direction, but rotation was not permitted. The left and right boundaries were free to translate, but not rotate. The lowest buckling load was found utilising the inbuilt linear buckling solver of COMSOL 5.2.

In all quasi-static studies reported in this work, a displacement was imposed on the upper and lower boundaries in the y direction, and the reaction force was measured on these boundaries. These boundaries (upper and lower) were free to translate in the x direction, but rotation was not permitted. The left and right boundaries were free to translate, but not rotate. In the studies relating to postbuckling initial imperfections were added to the lattice in the form of the first eigenmode, a measure of the magnitude of these imperfections is given in figure 5. These imperfections were found through linear buckling analysis and added to the lattice through the use of MeshPerturb 1.0 [57]. The addition of further imperfections in the form of higher eigenmodes did not make any significant difference to the results presented here.

For the measurements of the Poisson's ratio we follow the method of [31,33]: We used a quasi-static simulation, recording the positions of the nodes within the structure as the imposed displacement on the upper/lower boundaries was increased. The displacements of these nodes were then analysed to find the longitudanal and transverse strain, and therefore the Poisson's

ratio at that point in the loading procedure. The Poisson's ratio reported in figure 6 is the minimum observed during the loading procedure, typically immediately before the onset of localisation of deformations, as reported in the main text. The Poisson's ratio that was obtained through analysis of the displacements of a single unit cell towards the centre of the lattice was found to be representative of the structure.

Ethics. Nothing to declare

Data Accessibility. This work does not have any experimental data.

Authors' Contributions. DRK, LT and MD conceived the project. CZ performed initial analytic work. MD and DRK performed finite element work. DRK performed the analysis presented here and wrote the manuscript. All authors gave final approval for publication.

Competing Interests. We have no competing interests.

Funding. DRK acknowledges funding support from Academy of Finland and Aalto Science Institute. CZ acknowledges funding from Aalto Science Institute. LT acknowledges funding from Aalto Science Institute thematic program "Challenges in large geometric structures and big data".

References

1. P. M. Reis, H. M. Jaeger, M. van Hecke, *Extreme Mech. Lett.*, **5** 25 (2015)
2. T. J. Cui, D. Smith, R. Liu, *Metamaterials: Theory, Design, and Applications*, (Springer, New York, 2010)
3. M. Kadic, T. Buckmann, R. Schittny, M. Wegener, *Reports on progress in physics*. Physical Society (Great Britain) **76**, 126501 (2013)
4. C. Lv, D. Krishnaraju, G. Konjevod, H. Yu and H. Jiang, *Sci. Rep.*, **4**, 5979 (2014)
5. R. Lakes, *Science*, **235**, 1038 (1987)
6. A. E. H. Love, *A Treatise on the Mathematical Theory of Elasticity*, Dover Publications, New York, NY, USA 1944.
7. F. Song, J. Zhou, X. Xu, Y. Xu, and Y. Bai *Phys. Rev. Lett.*, **100**, 245502 (2008)
8. A. Pozniak, J. Smardzewski and K. Wojciechowski, *Smart Mater. Struct.*, **22** 084009 (2013)
9. K. Dudek, R. Gatt, L. Mizzi, M. Dudek, D. Attard, K. Evans and J. Grima, *Sci. Rep.*, **7** 46520 (2017)
10. A. Spagnoli, R. Brighenti, M. Lanfranchi, F. Soncini *Procedia Engineering*, **109** 410 (2015)
11. M. Schenk, S. D. Guest, *Proc. Nat. A. Sciences.*, **110** 3276 (2013)
12. S. Kamrava, D. Mousanezhad, H. Ebrahimi, R. Ghosh, A. Vaziri, *Sci. Rep*, **7** 46046 (2017)
13. Y. Tang, J. Yin, *Extreme Mech. Lett.*, In Press (2016)
14. S. Shan, S. H. Kang, Z. Zhao, L. Fang, K. Bertoldi, *Extreme Mech. Lett.*, **4**, 96 (2015)
15. H. M. A. Kolken, A. A. Zadpoor, *R. C. S. Adv.*, **7**, 5111 (2017)
16. J. Grima, A. Alderson and K. Evans, *Phys. Stat. Sol (b)*, **242** 561 (2005)
17. J. Grima, E. Manicaro, and D. Attard, *Proc. Royal Soc. A*, **467**, 439 (2011)
18. J. Grima, E. Chetcuti, E. Manicaro, D. Attard, M. Camilleri, R. Gatt, K. Evans, *Proc. Royal Soc. A*, rspa20110273 (2011)
19. F. Javid, E. Smith-Roberge, M. C. Innes, A. Shanian, J. C. Weaver, K. Bertoldi, *Sci. Rep.*, **5** 18373 (2015)
20. H. Mitschke, et al., *Int. J. Solids Structs.*, **100** 1 (2006)
21. C. Borcea, and I. Streinu, *Proc. Royal Soc. A*, **471** 20150033 (2015)
22. T. Hughes, A. Marmier and K. Evans, *Int J. Solids Struct.*, **47**, 1469 (2010)
23. R. Lakes, *Annual Review of Materials Research*, **47** 63 (2017)
24. K. Saxena, R. Das and E. Calius, *Adv. Eng. Mat.*, **18** 1847 (2016)
25. T. Frenzel, C. Findeisen, M. Kadic, P. Gumbsch, and M. Wegener, *Adv. Mat.*, **28** 5865 (2016)
26. P. Reis, *J. Appl. Mech* **82**, 111001 (2015)
27. D. Rayneau-Kirkhope and M. Dias, *Physics World*, **30** 25 (2017)
28. C. Coulais, E. Teomy, K. de Reus, Y. Shokef, M. van Hecke, *Nature*, **535** 529 (2016)
29. J. Shim, C. Perdigou, E. R. Chen, K. Bertoldi, P. M. Reis, *PNAS*, **109**, 5978 (2012)
30. J. Grima in *New Auxetic Materials*, Ph.D. Thesis, University of Exeter, UK 2000, Ch. 5
31. K. Bertoldi, P. Reis, S. Willshaw, T. Mullin, *Adv. Mat.*, **22**, 361 (2009)
32. T. Mullin, S. Deschanel, K. Bertoldi, M. Boyce, *Phys. Rev. Lett.*, **99** 084301 (2007).

33. S. Babaee, J. Shim, J. C. Weaver, E. R. Chen, N. Patel, K. Bertoldi *Adv. Mat*, **25**, 5044 (2013)
34. D. Mousanezhad, S. Babaee, H. Ebrahimi, R. Ghosh, A. S., Hamouda, K. Bertoldi, A. Vaziri, *Sci. Rep.*, **5**, 18306 (2015)
35. Y. He, Y. Zhou, Z. Liu, K. Liew, *Mat. Design*, **132**, 375 (2017)
36. Y. Chen, T. Li, F. Scarpa, L. Wang, *Phys. Rev. Appl.*, **7** 024012 (2017)
37. D. Rayneau-Kirkhope, M. A. Dias, *Extreme Mech. Lett.*, **9**, 11 (2016)
38. B. Haghpanah, J. Papadopoulos, D. Mousanezhad, H. Nayeb-Hashemi, A. Vaziri, *Proc. Royal Soc. A*, **470** 20130856 (2014)
39. V. Kapko, M. Treacy, M. Thorpe and S. Guest, *Proc. Royal Soc. A*, **465** 3517 (2009)
40. H. Mitschke, V. Robins, K. Mecke and G. Schroder-Turk, *Proc. Royal Soc. A*, **469**, 2149 (2012)
41. L. Gibson, M. Ashby, Cellular Solids: Structure and Properties, Cambridge University Press, Cambridge, UK, 1997
42. S. Guest and S. Pellegrino, *ASME Journal of Applied Mechanics*, **61**, 773 (1994)
43. M. Ashby, *Proc. Royal Soc. A*, **364** 15 (2006)
44. V. Deshpande, et al., *Acta Mater.*, **49** 1035 (2001)
45. J. T. B. Overvelde, K. Bertoldi, *J. Mech. Phys. Solids*, **64**, 351, (2014)
46. K. Ikeda, K. Murota, *Imperfect bifurcation in structures and materials: engineering use of group-theoretic bifurcation theory*, **149**, Springer Science & Business Media, 2010.
47. M. Dias, B. Audoly, *J. Mech. Phys. Solids* **62** 57 (2014)
48. M. Ohsaki and K. Ikeda, *Stability and Optimisation of Structures: Generalized Sensitivity Analysis*, Springer (New York) (2007) **62** 57 (2014)
49. S. Timoshenko and J. Gere, *Theory of Elastic Stability*, Dover Civil and Mechanical Engineering, Dover Publications, 2009
50. S. H. Kang, S. Shan, A. Kosmrlj, W. L. Nooduin, S. Shain, J. C. Weaver, D. R. Clarke, K. Bertoldi, *Phys. Rev. Lett.*, **112**, 098710 (2014)
51. B. Florijn, C. Coulais, M. van Hecke, *Phys. Rev. Lett.*, **113**, 175503 (2014)
52. M. Hanifpour, C. Peterson, M. Alava and S. Zapperi, Pre-print published 04 April 2017, https://arxiv.org/abs/1704.00943
53. K. Hammonds, V. Heine and M. Dove, *J. Phys. Chem. B*, **102**, 1759 (1998)
54. J. Grima, R. Jackson, A. Alderson and K. Evans, *Adv. Mat.*, **12**, 1912 (2000)
55. A. Vasiliev, Dmitriev, Y. Ishibashi and T. Shigenari, *Phys. Rev. B*, **65**, 094101 (2002)
56. COMSOL Inc., http://www.comsol.com/comsol-multiphysics last accessed 06 Feb 2017
57. S. K. Saha, M. L. Culpepper, MeshPerturb: MATLAB codes for mesh perturbation and automated pre and post processing of post-bifurcation analyses via COMSOL, http://hdl.handle.net/1721.1/86934 (2014) last accessed 06 Feb 2017.